

Two-center shell potential: Spectral fluctuations and an effective underlying classical dynamics

Debabrata Biswas

Theoretical Physics Division, Central Complex, Bhabha Atomic Research Centre, Bombay 400 085, India

Santanu Pal and Asis Chaudhuri

Variable Energy Cyclotron Centre, 1/AF Bidhan Nagar, Calcutta 700 064, India

(Received 20 April 1992)

The two-center shell potential is an example of a system that does not possess an obvious classical analog. We carry out a detailed study of the spectral measures and find, apart from other interesting details, a regular-irregular-regular transition in both the nearest-neighbor-spacing distribution as well as the spectral rigidity with a variation in the separation between the two nuclei. Moreover, the saturation of the spectral rigidity, together with an accurate prediction of its onset using the Fourier transform of the spectrum, clearly indicates that a "Gutzwiller-like" sum rule for the density of states does exist in this system.

PACS number(s): 03.65.Sq, 03.65.Ge, 05.45.+b

I. INTRODUCTION

Extensive studies on the fluctuations in the density of the quantal energy eigenvalues during the past decade have established the existence of universality classes [1] determined essentially by the nature of the underlying classical dynamics. Among the typical fluctuation measures used in these investigations are the nearest-neighbor level-spacing distribution $P(s)$ and the spectral rigidity Δ_3 . Their behavior is quite distinct for the two extreme cases of the classical flow. In the integrable case, the dynamics is regular and the quantum spectra exhibit fluctuations typical of a Poisson process. For chaotic systems, on the other hand, the fluctuations are close to those of the eigenvalues of random matrices reflecting the presence or absence of antiunitary symmetries. In the generic case, where the phase space is mixed, the statistics is intermediate. This present understanding is largely due to the successful applications [2,3] of the semiclassical periodic orbit theory [4] aided by certain classical [2,5] and semiclassical [3] sum rules.

The emphasis in these studies has, however, been on systems which possess a clear classical analog and are described by a scalar wave field. This made the interpretation of results largely unambiguous. The few numerical studies [6] on spectral measures in systems with multicomponent wave functions show a similar behavior. In their analytical work, Littlejohn and Flynn [7] succeeded in decoupling the wave components by extending WKB approximations to multicomponent wave fields and using Weyl transformations. This work thus showed that for each individual "polarization," there exists a classical Hamiltonian and the semiclassical description is given by a scalar wave. The presence of an underlying classical dynamics was indeed indicated by Biswas, Pal, and Chaudhuri [8] while studying the two-component wave functions in an axially symmetric system with spin-orbit coupling. Apart from a transition from regular to irregular in the nodal patterns and contour plots, regions of

unusually high probability density were observed analogous to the "scarred states" that show up in systems with a classical limit. In a subsequent publication, Littlejohn and Flynn [9] considered spin-orbit coupling semiclassically for integrable systems and obtained the classical Hamiltonian. In this paper, we shall seek further evidence of classical dynamics for the above two-component system [8] in both the integrable and chaotic regimes using the spectral rigidity Δ_3 .

Predictions of random matrix theories [10] on the spectral rigidity differ from numerical observations (at least for systems with few degrees of freedom) in an important aspect — $\Delta_3(L)$ saturates for values of L much larger than the characteristic outer scale in the spectrum (the inner scale is the mean spacing distribution). This, however, can be explained [3] by the periodic orbit theory (POT) which takes into account the underlying classical dynamics. The outer scale is in fact determined by the shortest periodic orbit which also dominates the saturation value of $\Delta_3(L)$. Thus, for the existence of an effective classical Hamiltonian in the two-center shell model, the spectral rigidity must saturate.

The eigenvalues can in fact be exploited to extract further information about the classical dynamics. A Fourier transform of the spectrum is known to reveal sharp peaks at the periods of the classical periodic orbits [11–14]. For a system without any obvious classical limit, such a behavior can well be misleading. Assuming for the moment that the peaks do correspond to the time periods; the smallest of these should give a value of the outer scale consistent with the saturation of the spectral rigidity.

Studies along these lines for the two-center shell model potential form an important aspect of our current investigations. In the two earlier studies on this system [6,7], the focus has been on the variation of the nearest-neighbor-level spacing distribution (NNLD) with a parameter that measures the separation R between the two centers (see Sec. II for details). A transition from Poisson statistic at $R=0$ to Gaussian orthonormal ensemble

(GOE) at intermediate values of R and back again to Poisson at large separations formed the chief observation. The histogram representation is, however, known to be inadequate since $P(s)$ depends sensitively on the bin size [15,16]. Further, important details get washed out [16]. We thus investigate the spacing distribution using more reliable techniques and find the emergence of interesting details both at small (as well as large) and intermediate separations. We also study the spectral rigidity in the region of universality and find that our conclusions are identical to those from the NNLD. For example, the variation of the fitting parameters follows similar patterns in both cases.

The paper is organized along the following lines. Section II contains a brief description of the two-center shell model potential. Studies on the variation of $P(s)$ and Δ_3 with R constitute Sec. III. In Sec. IV we seek further evidence of the existence of an effective underlying classical dynamics using the spectral rigidity. Discussions form the concluding section.

II. THE TWO-CENTER POTENTIAL

The two-center potential has often been used to model shape transitions in heavy-ion collisions. The total Hamiltonian of a single particle in the combined field of two axially symmetric harmonic oscillators centered at $z_1 < 0$ and $z_2 > 0$ (the position of the barrier is at the origin) joined smoothly by a neck (Fig. 1) and with a spin-orbit potential is given as [17]:

$$H = T + U + U_{SO} , \quad (1)$$

where

$$U_{\text{neck}} = \begin{cases} \frac{1}{2}M\{d_1\omega_{z_1}^2(z-z_1)^2 + g_1\omega_{\rho_1}^2\rho^2\}(z-z'_1)^2\Theta(z-z'_1) & \text{for } z < 0 \\ \frac{1}{2}M\{d_2\omega_{z_2}^2(z-z_2)^2 + g_2\omega_{\rho_2}^2\rho^2\}(z-z'_2)^2\Theta(z'_2-z) & \text{for } z > 0 \end{cases} \quad (5)$$

for $z'_1 < 0 < z'_2$. The parameters of Eq. (4) are obtained from the smooth matching conditions of the potential and are given as

$$\begin{aligned} \varepsilon &= U_1/U_2 , \\ z'_i &= z_i(1-\varepsilon)/\varepsilon , \\ d_i &= -\varepsilon^2/\{(1-\varepsilon)z_i^2\} , \\ g_1 &= \varepsilon^2(Q^2-1)(Q+1)/\{(1-\varepsilon)^2QR^2\} , \quad g_2 = -g_1/Q . \end{aligned} \quad (6)$$

The spin-orbit potential is evaluated in the same way as in Ref. [18].

For a given R , Q , ε and δ , only one of the frequencies remains to be fixed for a complete description of the model. Considering a system of A nucleons, we shall obtain the frequency ω_{ρ_1} by requiring [18] the volume under the equipotential surface $V_0 = M\omega_0^2R_0^2/2 = W_0 = (4\pi/3)R_0^3$, where $R_0 = 1.2249 A^{1/3}$ fm and $\hbar\omega_0 = 41$ MeV $A^{-1/3}$.

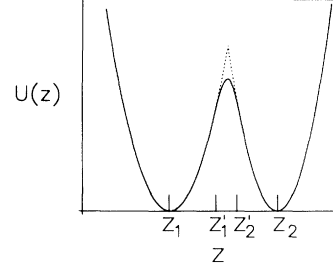


FIG. 1. The two-center oscillator potential along the z axis. The two centers are at z_1 and z_2 and the barrier is at the origin. The barrier heights with (full line) and without (dotted line) the neck potential are U_1 and U_2 , respectively.

$$U = U_{\text{HO}} + U_{\text{neck}} , \quad (2)$$

$$U_{\text{HO}}(\rho, z) = \begin{cases} \frac{1}{2}M\omega_{\rho_1}^2\rho^2 + \frac{1}{2}M\omega_{z_1}^2(z-z_1)^2 & \text{for } z < 0 \\ \frac{1}{2}M\omega_{\rho_2}^2\rho^2 + \frac{1}{2}M\omega_{z_2}^2(z-z_2)^2 & \text{for } z > 0 , \end{cases} \quad (3)$$

ρ and z being the cylindrical coordinates. The above potential is essentially characterized by

$$\begin{aligned} R &= z_2 - z_1 , \\ Q &= \omega_{\rho_2}/\omega_{\rho_1} , \\ \delta &= \omega_{z_1}/\omega_{\rho_1} = \omega_{z_2}/\omega_{\rho_2} , \end{aligned} \quad (4)$$

giving $z_1 = -QR/(1+Q)$ and $z_2 = R/(1+Q)$. The neck potential joining the two oscillators of Eq. (2) is defined as [17]

In what follows, we shall consider an $A=260$ system with $\delta=1$ and $\varepsilon=0.8$. The asymptotic value of Q is taken as 1.1695 which corresponds to an asymptotic mass asymmetry of 1.6, thereby placing two nuclei of masses 160 and 100 at z_1 and z_2 , respectively, for large separations. We shall be concerned with the neutron single-particle levels in the following calculations.

In the absence of neck and spin-orbit potentials, the system is clearly separable and can be assigned good quantum numbers. The eigenfunctions are thus regular as one would expect. The introduction of the neck potential leads to nonseparability in the region $z'_1 < z < z'_2$. Our numerical investigations show that the nature of quantum-mechanical energy eigenfunctions does not change drastically even at this stage. The presence of the spin-orbit potential, however, has significant effects. The eigenfunctions ψ_n are now of the form

$$\psi_n = \phi_n^1(\rho, z)|\uparrow\rangle + \phi_n^2(\rho, z)|\downarrow\rangle . \quad (7)$$

As R increases from zero, the individual spatial components ϕ_n^i ($i=1,2$) of generic wave functions undergo a regular-irregular-regular transition [9] as in the nearest-neighbor-spacing distribution [6,7]. States with unusually high probability density in certain regions also appear [9] and are similar to the scarred states seen in systems with a classical limit.

The eigenvalues used for the study of spectral fluctuations in Secs. III and IV have been obtained by diagonalizing the Hamiltonian in a basis discussed in Ref. [18]. A total of 464 states have been used and the convergence for the first 150 eigenvalues was found to be excellent. The levels have been unfolded using a polynomial of degree 8 and the mean density is found to be unity. The unfolded levels are denoted by ε_n . For evaluating the spacing distribution in the following section, we have excluded the first 20 levels.

III. VARIATION OF $P(s)$ AND Δ_3 WITH R

In the following, we shall carry out a detailed study of the nearest-neighbor-spacing distribution $P(s)$ and the spectral rigidity Δ_3 with an emphasis on their variation with the separation R of the two centers. Apart from the regular-irregular-regular transition already observed by Milek, Norenberg, and Rozmej [6] and Pal and Chaudhuri [6] in the NNLD, the emergence of finer details leads us to generalizations of the Brody [19] and Berry-Robnik [20] distributions for $P(s)$ in order to obtain better fits. Studies on the spectral rigidity in this section are for the sake of a comparative study of the variation in the fit parameter as well as for completeness.

The nearest-neighbor level-spacing distribution, $P(s)$ is defined such that $P(s)$ is the probability of finding pairs $\{\varepsilon_i, \varepsilon_{i+1}\}$ with spacing between s and $s+ds$. Since the normal histogram representation depends sensitively on the bin size, we expand $P(s)$ in terms of Laguerre polynomials [15,16] $L_n(s)$:

$$P(s) = \frac{1}{N} \sum_{i=1}^N \delta(s - s_i) = \sum_n C_n L_n(s) e^{-s}, \quad (8)$$

$$\Delta_3(L) = \begin{cases} L/15, & \text{integrable} \\ \ln(L)/\pi^2 - 0.00695, & \text{chaotic with time reversal} \\ \ln(L)/2\pi^2 - 0.059, & \text{chaotic without symmetry} \end{cases} \quad (12)$$

The averaging is performed over an energy interval large compared to L_{\max} . The second expression of Eq. (12) holds for other antiunitary symmetries as well.

Figure 2 shows plots of the nearest-neighbor-spacing distribution $P(s)$ for values of R in the range 0–18 fm in comparison with the Poisson and GOE results. The degree of level clustering reduces with the separation and vanishes altogether at $R=10$. It increases again thereafter and, for large separations, attains a value close to that at $R=0$. There is also a similar regular-irregular-regular transition in the overall distribution as the plot indicates.

Certain interesting details appear as well. At $R=0$,

where $N+1$ is the total number of levels and C_n 's are the coefficients to be determined. Convergence is found to be excellent with a 25-term expansion and is easily checked by plotting the cumulative distribution, $\int_0^s P(s') ds'$.

For generic integrable systems where the contours in action space are curved [3] and the periodic orbit actions are nondegenerate [21], $P(s)$ is the Poisson distribution e^{-s} , indicating a clustering of levels. This is the only result for NNLD based on the periodic orbit theory. For chaotic systems with time-reversal invariance (or other antiunitary symmetry), numerical explorations on a number of systems [1] show that $P(s)$ is well approximated by the Wigner distribution,

$$P(s) = \frac{\pi}{2} s e^{-(\pi^2 s^2/4)}, \quad (9)$$

while for those without any symmetry, the distribution

$$P(s) = \frac{32}{\pi^2} s^2 e^{-(4s^2/\pi^2)} \quad (10)$$

is found to be appropriate [22]. Equation (10) closely approximates the result for the Gaussian unitary ensemble (GUE). Both cases are characterized by a repulsion between neighboring levels in sharp contrast to the clustering observed in generic integrable systems.

The spectral rigidity $\Delta_3(L)$ is the first measure for which expressions have been obtained using the periodic orbit theory for both the integrable and chaotic case. It is defined as

$$\Delta_3(L) = \left\langle \min_{a,b} \frac{1}{L} \int_{-L/2}^{+L/2} [N(x+\varepsilon) - a - b\varepsilon]^2 d\varepsilon \right\rangle \quad (11)$$

and is a measure of the average least-squares deviation of the integrated density of “unfolded” states, $N(\varepsilon)$, from the best fitting straight line $a + b\varepsilon$. For values of L in the range $1 < L \ll L_{\max}$ (a characteristic outer scale determined by the shortest periodic orbit—for details, see Sec. IV), $\Delta_3(L)$ displays universality, the nature of which depends on the underlying classical dynamics. Thus

the potential $U(\rho, z)$ is a pure harmonic oscillator. In the absence of the spin-orbit coupling therefore, the system belongs to the nongeneric category [2] of integrable systems and hence should display no universality. The presence of U_{SO} pushes the distribution towards a Poisson. However, there are oscillations as well and these are characteristic of Hamiltonians having terms that are weakly nonlinear terms in actions [23]. A similar phenomenon occurs at $R=18$ as well. Thus the effect of spin-orbit coupling at these separations is identical to an addition of weak nonlinear terms in the harmonic oscillator Hamiltonian.

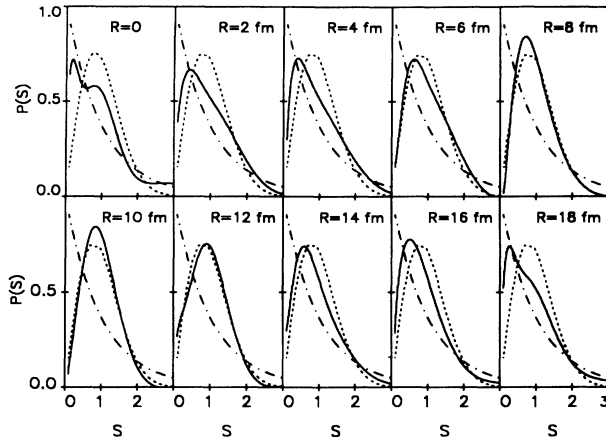


FIG. 2. The nearest-neighbor-spacing distribution $P(s)$ for the two-center shell potential (continuous curve) for various values of the parameter R . The Poisson and Wigner distributions are also shown. A regular-irregular-regular transition is evident.

In order to get a more quantitative picture of the spacing distribution at $R=0$ and 18, we have obtained the best-fit Brody distribution [19]

$$P(s) = As^\omega \exp(-\alpha s^{1+\omega}), \quad (13)$$

where $\alpha = [\Gamma((\omega+2)/(\omega+1))]^{\omega+1}$, $A = (1+\omega)\alpha$, and parametrized by ω . The two extreme cases at $\omega=0$ and 1 are Poisson and GOE results, respectively. The plots are shown in Fig. 3. The fits, though far from satisfactory, give an indication of the closeness to the Poisson distribution. The parameter values are 0.287 at $R=0$ and 0.309 at $R=18$.

At $R=10$ fm where the repulsion is maximum, the distribution shows considerable deviations from the GOE result. The fits to Brody and Berry-Robnik distributions are, however, good but with parameter values larger than unity leading to problems in interpretations. We have thus generalized the ideas of Brody and Berry-Robnik in order to get a transition from the Poisson distribution to that of GUE with a variation in parameter. We only give the final results since the algebra is straightforward. The generalized Brody distribution (Poisson \rightarrow GUE) reads

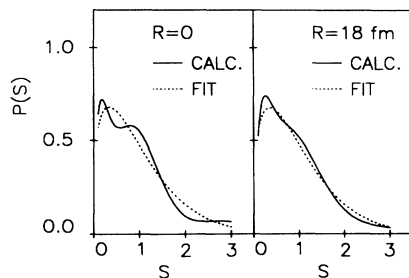


FIG. 3. The numerically obtained $P(s)$ at $R=0$ and 18 fm (continuous curve) along with the best-fit Brody distribution of Eq. (13).

$$P(s) = As^{2\omega} \exp(-\alpha s^{1+\omega}), \quad (14)$$

where $\alpha = [1/\Gamma((2\omega+1)/(\omega+1))]^{\omega+1}$ and $A = (1+\omega)\alpha^2$. The $\omega=0$ and 1 limits are the Poisson and GUE results, respectively. The Berry-Robnik distribution generalized to interpolate between the Poisson and GUE result can similarly be expressed as

$$P(s) = \frac{32}{\pi^2} [\rho_1^4 \rho_2^2 \{I_1 - sI_2\} \exp(-\rho_1 s) + 2\rho_2^4 \rho_1 I_2 \exp(-\rho_1 s) + \rho_2^4 s^2 \exp(-\rho_1 s) \exp(-4\rho_2^2 s^2/\pi)], \quad (15)$$

where

$$I_1 = \int_s^\infty x^2 \exp(-4\rho_2^2 x^2/\pi) dx,$$

$$I_2 = \int_s^\infty x^3 \exp(-4\rho_2^2 x^2/\pi) dx,$$

and $\rho_1 + \rho_2 = 1$. The Poisson result is obtained for $\rho_1 = 1$ and the GUE result for $\rho_2 = 1$.

Figure 4 shows the best fit to the numerically obtained values of $P(s)$ at $R=10$ fm with Eqs. (14) and (15). The generalized Brody distribution gives an excellent approximation for all values of s with the parameter $\omega=0.794$. Equation (15), however, shows a poor fit due to the fact that for values of $\rho_1 < 1$, $P(s)$ has nonzero value at $s=0$. These results have a great significance in view of our conclusions in the following section. If one is to accept the presence of an effective underlying classical dynamics, the presence of a substantial GUE component does indicate the absence of antiunitary symmetries in the classical system.

The regular-irregular-regular transition can be seen in the spectral rigidity as well. We have evaluated Δ_3 for $2 \leq L \leq 5$ so as to remain in the region of universality. The averaging has been carried out in an interval $[\varepsilon - \Delta\varepsilon, \varepsilon + \Delta\varepsilon]$, where $\varepsilon=85$ and $\Delta\varepsilon=65$. Our results are displayed in Fig. 5 for values of the separation R considered in Fig. 2. The gradual shift towards the GOE result is evident as R increases from zero. Moreover, for $6 \leq R \leq 10$, the rigidity distinctly falls below the GOE curve (but remains above GUE values) before finally registering a shift towards the Poisson result.

A plot of the variation in the best-fit parameter with R shows the transition more clearly. For the nearest-

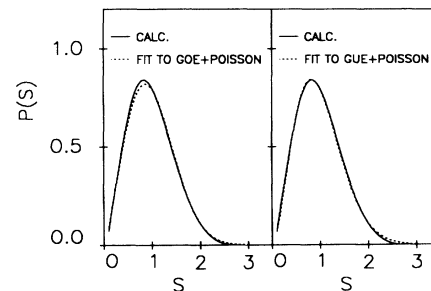


FIG. 4. A comparative study of the fits at $R=10$ fm using the Brody (Poisson plus GOE) and Brody (Poisson plus GUE) distributions. The parameter ω exceeds unity in the former case.

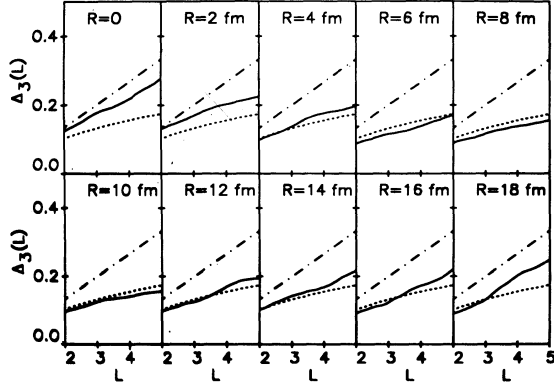


FIG. 5. The numerically obtained spectral rigidity $\Delta_3(L)$ for various R values (continuous curve) along with Poisson ($L/15$) and GOE predictions.

neighbor-spacing distribution, we have considered Eqs. (13)–(15) as well as the Berry-Robnik distribution [20] for the Poisson \rightarrow GOE case,

$$P(s) = \rho_1^2 e^{-\rho_1 s} \operatorname{erfc}(\sqrt{\pi} \rho_2 s / 2) + (2\rho_1 \rho_2 + \pi \rho_2^3 s / 2) e^{-(\rho_1 s + \pi \rho_2^2 s^2 / 4)}, \quad (16)$$

where $\rho_1 + \rho_2 = 1$ and $\rho_1 = 1$ gives the Poisson distribution while $\rho_1 = 0$ is the Wigner distribution of Eq. (9).

For the spectral rigidity, arguments similar to those of Berry and Robnik for $P(s)$ lead to one-parameter distributions displaying a transition from Poisson ($L/15$) to

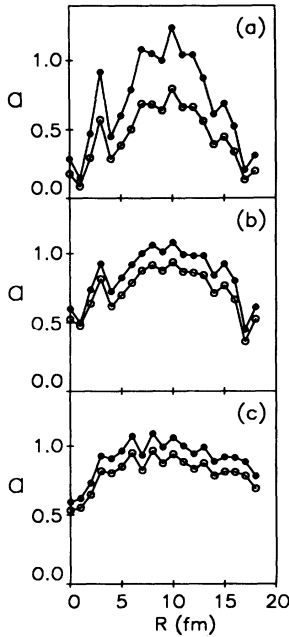


FIG. 6. Parameter variation with R . Fits to $P(s)$ are shown in (a) and (b) for the Brody and Berry-Robnik distributions while (c) shows fits to $\Delta_3(L)$. Dots denote a Poisson plus GOE form while open circles are for the Poisson plus GUE form of the fitting function.

GOE or GUE as the case may be. Thus

$$\Delta_3(L; \rho_1) = \Delta_3^P(L\rho_1) + \Delta_3^G(L\rho_2), \quad (17)$$

where $\rho_2 = 1 - \rho_1$ and the superscripts P and G refer to the Poisson and GOE-GUE expressions, respectively.

The variation of the fitting parameter (ρ_2 or ω , both of which measure the degree of irregularity in the system) with R is displayed in Fig. 6 for both the nearest-neighbor-spacing distribution [Figs. 6(a) and 6(b)] and the spectral rigidity [Fig. 6(c)]. (The parameter has been denoted by a in the figure for uniformity.) In all three cases, the trend is similar, indicating a regular-irregular-regular transition. However, for R in the interval (6,10), the fitting parameter for the Poisson \rightarrow GOE transition in each case exceeds unity as mentioned earlier leading to problems in interpretation. Fits using the Poisson \rightarrow GUE transition give a more meaningful result and in some cases ($R = 10$ fm for Brody type) the agreement is indeed excellent.

IV. EXISTENCE OF AN EFFECTIVE UNDERLYING CLASSICAL DYNAMICS

The existence of universalities in the spectral measures is now known to be related to certain collective properties of the periodic orbits belonging to the underlying classical system. Though the presence of the spin-orbit interaction in the present Hamiltonian makes it difficult to identify an obvious classical analog, its existence has nevertheless been demonstrated analytically by Littlejohn and Flynn for multicomponent systems in general [7] and integrable systems with spin-orbit coupling in particular [9]. Thus it would be of interest to explore the signatures of classical dynamics in the present system as an exact analytical form of the classical Hamiltonian for nonintegrable systems with spin-orbit coupling is yet to be obtained.

The saturation of the spectral rigidity for large L is one of the remarkable predictions of the periodic orbit theory [3]. It has been observed in a number of systems, both integrable [24] as well as chaotic [25] and the saturation value itself was found to have excellent agreement with theoretical expectations. Random matrix theories, however, do not predict such a behavior. The saturation of $\Delta_3(L)$ is thus a clear signature of an underlying classical system.

The analysis of $\Delta_3(L)$ in terms of periodic orbits has

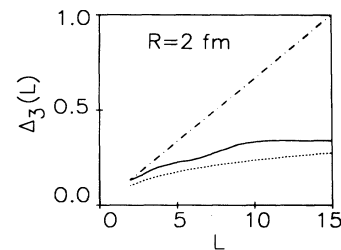


FIG. 7. The spectral rigidity at $R = 2$ fm shows saturation near $L = 15$.

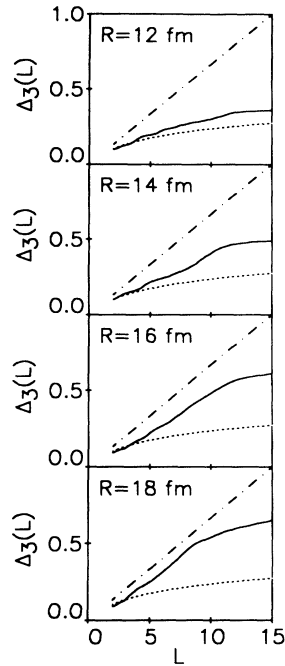


FIG. 8. As in Fig. 7 for $R = 12, 14, 16$ and 18 fm. The plots denote a monotonic increase in the value of L_{\max} for $R > 12$ fm (see Table I also).

been carried out in considerable detail by Berry [3]. Two relevant scales in the spectrum clearly emerge. The first (and the more obvious) is the inner scale given by the mean spacing between neighboring levels while the second or the outer scale, denoted by L_{\max} , is determined essentially by the shortest periodic orbit. Thus

$$L_{\max} = \frac{h d_{\text{av}}(E)}{T_{\min}}, \quad (18)$$

where $d_{\text{av}}(E)$ is the mean density at the energy E and T_{\min} is the shortest time period of the closed orbit.

For $L > L_{\max}$, all periodic orbits have a constant contribution leading to the saturation of $\Delta_3(L)$. Moreover, the saturation value is dominated by the shortest periodic orbit.

We have evaluated $\Delta_3(L)$ for values of L in the interval $[0, 15]$ for the R values considered earlier. Saturation, however, sets in clearly for $R = 2$ alone. Our results are

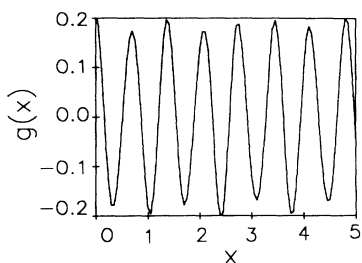


FIG. 9. The function $g(x)$ of Eq. (19) for $R = 2$ fm. The position of the first peak, x_{\min} , is used to evaluate L_{\max} in Table I.

TABLE I. Values of level density $d_{\text{av}}(E)$ and the outer scale L_{\max} for various values of the parameter R .

R	$d_{\text{av}}(E)$	$L_{\max} = 2\pi d_{\text{av}}/x_{\min}$
0	1.987	19.2
2	1.902	17.0
4	1.845	17.8
6	1.809	18.9
8	1.810	20.7
10	1.830	20.9
12	1.870	21.4
14	1.963	22.4
16	2.052	23.4
18	2.121	24.3

displayed in Fig. 7. For $R = 12, 14, 16$, and 18 fm, the quantity L_{\max} clearly increases (Fig. 8) and the saturation at $L = 15$ becomes less prominent.

The eigenvalues can indeed be used to extract further information about the classical dynamics. A Fourier transform of the spectrum is known to reveal sharp peaks at the periods of the classical periodic orbits [11–14]. For a system without any obvious classical limit, such a behavior can well be misleading. Assuming for the moment that the peaks do correspond to the time periods, the smallest of these should give a value of the outer scale consistent with the saturation of the spectral rigidity. We have thus evaluated the function

$$g(x) = \sum_n \cos(E_n x) \exp(-E_n^2 \beta), \quad (19)$$

with $\beta = 0.02$. A total of 165 eigenvalues have been used in the sum and the value of β is chosen so as to minimize the errors due to the truncation. Figure 9 shows a plot of $g(x)$ for $R = 2$ fm. The position of the first peak together with Eq. (18) and the appropriate mean density evaluated numerically give a value of $L_{\max} = 17$. This is indeed consistent with our observations in Fig. 7 where saturation seems to set around $L = 15$. We have also evaluated L_{\max} for other values of R as shown in Table I. It clearly registers an increase for $R > 12$ which is again consistent with our observations of Fig. 8.

We thus have a clear indication of the existence of an effective underlying classical dynamics which determines the spectral fluctuations.

V. DISCUSSIONS AND SUMMARY

In the preceding sections, we have carried out a detailed investigation of certain spectral measures in the two-center shell potential, parametrized by the separation R . The system clearly does not possess any obvious classical analog due to the spin-orbit interaction but nevertheless has fluctuations similar to those in systems with a classical limit. We have further explored the signatures of an effective underlying classical dynamics influencing the spectrum. Our conclusion corroborates the analytical work of Littlejohn and Flynn [7,9] and can be stated as follows.

“The saturation of the spectral rigidity, together with an accurate prediction of its onset using the Fourier

transform of the spectrum, clearly indicates that a Gutwillzer-like sum rule for the density of states [$d(E) = d_{av}(E) + d_{osc}(E)$ where $d_{osc}(E)$ is an infinite sum of oscillatory contributions] does exist in this system. In other words, an effective underlying classical dynamics does influence the spectrum.”

We have also looked at the variation of $P(s)$ and $\Delta_3(L)$ with R . A regular-irregular-regular transition for small-intermediate-large R occurs in both measures. Two re-

markable facts emerge.

(a) For intermediate separations (typically at $R = 10$ fm), the fluctuations are closer to those of GUE indicating the absence of (antiunitary) symmetries in the effective underlying classical dynamics though the full Hamiltonian does have time-reversal invariance.

(b) At $R = 0$ fm, the effect of the spin-orbit coupling is similar to the presence of weak nonlinear terms (in action variables) in the harmonic oscillator Hamiltonian.

-
- [1] O. Bohigas and M.-J. Giaconni, in *Quantum Chaos and Statistical Nuclear Physics*, edited by T. H. Seligman and H. Nishoka, Lecture Notes in Physics Vol. 263 (Springer-Verlag, Berlin, 1986).
- [2] M. V. Berry, and M. Tabor, Proc. R. Soc. London Ser. A **356**, 375 (1977).
- [3] M. V. Berry, Proc. R. Soc. London Ser. A **400**, 229 (1985).
- [4] M. C. Gutzwiller, J. Math. Phys. **11**, 1791 (1970); **12**, 343 (1971); R. Balian and C. Bloch, Ann. Phys. (NY) **60**, 401 (1970); **64**, 371 (1971).
- [5] J. H. Hannay and A. M. Ozorio de Almeida, J. Phys. A **17**, 3429 (1984).
- [6] B. Milek, W. Norenberg, and P. Rozmej, Z. Phys. A **334**, 233 (1989); S. Pal and A. K. Chaudhuri, Nucl. Phys. A **537**, 237 (1991); C. H. Lewenkopf, M.C. Nemes, V. Marvulle, M. P. Pato, and W. F. Wreszinski, Phys. Lett. A **155**, 113 (1991).
- [7] R. G. Littlejohn and W. G. Flynn, Phys. Rev. A **44**, 5239 (1991).
- [8] D. Biswas, S. Pal, and A. K. Chaudhuri, Phys. Rev. A **45**, 6185 (1992).
- [9] R. G. Littlejohn and W. G. Flynn, Phys. Rev. A **45**, 7697 (1992).
- [10] M. L. Mehta, *Random Matrices* (Academic, New York, 1967).
- [11] D. Wintgen, Phys. Rev. Lett. **58**, 1589 (1987).
- [12] M. Seiber and F. Steiner, Physica D **44**, 248 (1990).
- [13] D. Biswas, M. Azam, and S. V. Lawande, Phys. Rev. A **44**, 4911 (1991).
- [14] D. Biswas, M. Azam, Q. V. Lawande, and S. V. Lawande, J. Phys. A **25**, L297 (1992).
- [15] A. Hönl and D. Wintgen, Phys. Rev. A **39**, 5642 (1989).
- [16] D. Biswas, Phys. Rev. A **44**, 2429 (1991).
- [17] A. Lukasiak, W. Cassing, and W. Norenberg, Nucl. Phys. A **246**, 181 (1984).
- [18] J. Maruhn and W. Greiner, Z. Phys. A **251**, 431 (1972).
- [19] T. A. Brody, Lett. Nuovo Cimento **7**, 482 (1973).
- [20] M. V. Berry and M. Robnik, J. Phys. A **17**, 2414 (1984).
- [21] D. Biswas, M. Azam, and S. V. Lawande, J. Phys. A **24**, 1825 (1991).
- [22] M. V. Berry and M. Robnik, J. Phys. A **19**, 649 (1986).
- [23] D. Biswas, S. Sinha, and S. V. Lawande, Phys. Rev. A **46**, 2649 (1992).
- [24] G. Casati, B. V. Chirikov, and I. Guarneri, Phys. Rev. Lett. **54**, 1350 (1985).
- [25] R. Aurich and F. Steiner, Physica D **43**, 155 (1990).